Remote Sensing of Environment 219 (2018) 1–14

Contents lists available at ScienceDirect

Remote Sensing of Environment

journal homepage: www.elsevier.com/locate/rse

SMAP soil moisture improves global evapotranspiration

Adam J. Purdy[a,b,*], Joshua B. Fisher[b], Michael L. Goulden[a], Andreas Colliander[b], Gregory Halverson[b], Kevin Tu[c], James S. Famiglietti[a,b]

[a] Department of Earth System Science, University of California, Irvine, CA 92697, USA
[b] Jet Propulsion Laboratory, California Institute of Technology, Pasadena, CA 91109, USA
[c] Dupont Pioneer, IA, USA

ARTICLE INFO

Keywords:
Evapotranspiration
Soil moisture
Hydrology
Evaporation
Transpiration
SMAP
MODIS

ABSTRACT

Accurate estimation of global evapotranspiration (ET) is essential to understand water cycle and land-atmosphere feedbacks in the Earth system. Satellite-driven ET models provide global estimates, but many of the ET algorithms have been designed independently of soil moisture observations. As water for ET is sourced from the soil, incorporating soil moisture into global remote sensing algorithms of ET should, in theory, improve performance, especially in water-limited regions. This paper presents an update to the widely-used Priestley Taylor-Jet Propulsion Laboratory (PT-JPL) ET algorithm to incorporate spatially explicit daily surface soil moisture control on soil evaporation and canopy transpiration. The updated algorithm is evaluated using 14 AmeriFlux eddy covariance towers co-located with COsmic-ray Soil Moisture Observing System (COSMOS) soil moisture observations. The new PT-JPL_{SM} model shows reduced errors and increased explanation of variance, with the greatest improvements in water-limited regions. Soil moisture incorporation into soil evaporation improves ET estimates by reducing bias and RMSE by 29.9% and 22.7% respectively, while soil moisture incorporation into transpiration improves ET estimates by reducing bias by 30.2%, RMSE by 16.9%. We apply the algorithm globally using soil moisture observations from the Soil Moisture Active Passive Mission (SMAP). These new global estimates of ET show reduced error at finer spatial resolutions and provide a rich dataset to evaluate land surface and climate models, vegetation response to changes in water availability and environmental conditions, and anthropogenic perturbations to the water cycle.

1. Introduction

Water movement from land to the atmosphere, or evapotranspiration (ET), is an integral part of earth's ecological and climate systems. This process links the water, carbon, and energy cycles in the earth system. Therefore, accurate observations of ET facilitate detection of the human fingerprint on the water cycle and surface energy budget (Lo and Famiglietti, 2013; Sorooshian et al., 2011), studies on land-atmosphere feedbacks related to heat wave intensity (Miralles et al., 2014), quantification of agricultural and ecosystem water use (Allen et al., 2007; Anderson et al., 2011; Goulden et al., 2012; Goulden and Bales, 2014), identification of droughts where plants may become vulnerable to other biotic stressors and potential mortality (Anderson et al., 2013; McDowell, 2011; Mu et al., 2013), and provide benchmarks to evaluate and improve parameterizations in land surface models (Mueller et al., 2013; Rodell et al., 2011). With increasing global temperatures and the subsequent greater atmospheric capacity for water vapor, ET may accelerate with the water cycle and alter global water distribution making certain regions drier (*Syed et al.*, 2010; *Huntington*, 2006). As land begins to dry, (Greve and Seneviratne, 2015; Jung et al., 2010) quantifying where and to what degree reductions in water availability limits ET becomes increasingly important.

Remote sensing algorithms are an effective way to derive observationally-constrained ET estimates at the necessary spatiotemporal resolutions to support earth observations (Fisher et al., 2017, 2008; Miralles et al., 2011; Mu et al., 2011; Su, 2002). Multiple manuscripts have reviewed the state and needs for ET remote sensing (Fisher et al., 2017; Wang and Dickinson, 2012) and one common theme across many of these remote sensing approaches is a limited or absent representation of soil moisture. Of the ET remote sensing algorithms, few approaches remain both physically defensible and globally applicable without reliance on data assimilation and prognostic land surface models. One model that lacks soil moisture representation and fits the aforementioned description is the Priestley-Taylor Jet Propulsion Laboratory (PT-JPL) ET model.

The PT-JPL ET model, a widely used remote sensing retrieval

* Corresponding author at: Department of Earth System Science, University of California, Irvine, CA 92697, USA.
E-mail address: ajpurdy@uci.edu (A.J. Purdy).

https://doi.org/10.1016/j.rse.2018.09.023
Received 8 December 2017; Received in revised form 20 September 2018; Accepted 25 September 2018

algorithm, has outperformed many models for the majority of globally distributed eddy covariance towers within model inter-comparison studies achieving both high explanation of variance and low error (Ershadi et al., 2014; Michel et al., 2016; Vinukollu et al., 2011). Despite a strong performance in these studies, the PT-JPL algorithm lacks soil moisture control and is restricted by its dependence on a combination of atmospheric conditions and vegetation characteristics to represent surface conditions. These limitations become especially evident in regions where the coarse near surface air temperature and water vapor pressure deviate from the underlying surface soil water availability at fine temporal frequencies, in areas with highly heterogeneous land covers, in areas of active land management, or in regions prone to atmospheric advection conditions. Therefore, incorporating soil moisture observations has great potential to address these limitations and improve global ET estimates but large challenges exist.

There are two main challenges to improve global estimates of ET using soil moisture: 1) observing accurate integrated values of soil moisture; and, 2) appropriately modeling how limitations from soil moisture interact with other environmental constraints to quantify ET.

The launch of the Soil Moisture Active Passive (SMAP) satellite (2015) addresses the first challenge through providing global soil moisture observations (Entekhabi et al., 2010). The SMAP mission has leveraged lessons from other global soil moisture observing satellites, such as the Advanced Microwave Scanning Radiometer- EOS (Njoku et al., 2003) and the Soil Moisture Ocean Salinity (Kerr et al., 2016) satellites to detect and mitigate potential radio frequency interference and provide observations at relatively high spatio-temporal [9–36 km, 3-daily] resolutions at a depth [5-cm] applicable to improve modeled ET (Johnson et al., 2016; Mohammed et al., 2016; Oliva et al., 2012; Piepmeier et al., 2014). These observations have been extensively evaluated as part of a rigorous calibration and validation campaign and shown to be within mission accuracy requirements (unbiased RMSE < 0.04 $cm^3 cm^{-3}$) and thus capable of supporting improvements to global ET quantification (Colliander et al., 2017). Additionally, despite only providing surface soil moisture observations, recent *in situ* analyses have shown that surface soil moisture provides similar amounts of predictive information as rooting depth soil moisture for latent heat quantification (Qiu et al., 2016).

To address the second challenge, model testing and updates needs to be done with coterminous observations of meteorological conditions, soil moisture, and ET. Observations of soil moisture and ET are made globally in distributed networks of eddy covariance (EC) towers as part of FLUXNET and AmeriFlux networks (Baldocchi et al., 2001). However, sites often include measurements of soil moisture at only 1–4 points and these points may misrepresent actual land surface conditions within the EC footprint making model parameterization and calibration difficult. Fortunately, a new observation network from the COsmic-ray Soil Moisture Observing System (COSMOS) provides integrated observations at similar scales to EC tower footprints (Zreda et al., 2012). EC observations of water and energy exchange at the earth's surface co-located with integrated soil moisture observations provide a valuable dataset to compliment satellite observations of environmental variables necessary to test and evaluate ET models (Baldocchi et al., 2001).

Generally, land surface and remote sensing models relate the amount of ET to water availability and the atmospheric demand for ET, but vary to what degree and at what point water availability limits and eventually prevents ET. Various adaptations of soil moisture normalized by soil properties to compute the relative extractable water (REW) have been applied to limit transpiration [Fig. S1, Table S1]. Yet, soil moisture is just one of many environmental variables that limits the maximum stomatal conductance, as temperature and vapor pressure extremes have been found to regulate transpiration (Fisher et al., 2008; Jarvis and Mcnaughton, 1986; Monteith, 1965; Mu et al., 2011; Novick et al., 2016). Therefore, modeling approaches that have adopted REW-based stressors are often applied in series with other scalar stressors, such as temperature and vapor pressure, to reduce potential ET based on sub-optimal environmental limitations (Fisher et al., 2008; Jin et al., 2011; Miralles et al., 2011). However, plant access to soil moisture varies with rooting depth and much uncertainty exists with the role deep roots play in mitigating limitations from soil water availability during drought (Schenk and Jackson, 2002). Plant type, canopy height and aboveground biomass provide indicators of rooting depth and the potential to access to deeper soil water (Canadell et al., 1996; Fan et al., 2017; Jackson et al., 1999). Miralles et al. (2011) postulate taller vegetation is less sensitive to soil water deficits compared to shorter canopy plants due to deep rooting potential to alleviate plants from seasonal drought conditions (*i.e.*, when precipitation occurs outside of the of summer maximum atmospheric demand). Recent global observations of canopy height create an opportunity to further inform plant sensitivity to environmental conditions (Simard et al., 2011).

We present an update to the PT-JPL algorithm by incorporating explicit surface soil moisture constraint from SMAP to model ET globally. To address previous model parameterization limitations, we use integrated *in situ* observations of soil moisture and ET to implement soil moisture control within the PT-JPL model. Then, we apply the new PT-JPL_{SM} model globally using soil moisture data from the Soil Moisture Active Passive mission (SMAP). The following sections will provide: (1) a description of the PT-JPL algorithm with updates detailing soil moisture constraints on evaporation and transpiration, (2) details on the datasets used in this study, (3) results evaluating the updated PT-JPL_{SM} model compared to the original PT-JPL model using eddy covariance towers from Ameriflux and globally using satellite datasets, and (4) discussion on the implications of soil moisture on global ET quantification improvement.

2. PT-JPL algorithm

2.1. PT-JPL ET algorithm

The Priestley Taylor-Jet Propulsion Laboratory (PT-JPL) ET algorithm applies ecophysiological constraints to model reductions of ET from the atmospheric potential ET due to sub-optimal environmental conditions (Fisher et al., 2008). The model incorporates a variety of data sources from satellite observations and reanalysis datasets [Fig. 1; Table 1]. Potential ET, or latent energy *LE*, is computed using the Priestley-Taylor model:

$$PET = \alpha \frac{\Delta}{\lambda(\Delta + \gamma)}(R_N - G) \tag{1}$$

where PET [$mm\ day^{-1}$] is the potential ET based on temperature and radiation, α is the Priestley-Taylor coefficient that is set to 1.26, Δ is the slope of the saturated vapor-pressure relationship [$kPa\ ^\circ C^{-1}$], and γ is the psychrometric constant [$kPa\ ^\circ C^{-1}$], and R_N is the net radiation [$W\ m^{-2}$], G is the ground heat flux [$W\ m^{-2}$], and λ is the latent heat of vaporization [$MJ\ kg^{-1}$] (Priestley and Taylor, 1972). The water cycle and energy cycle are linked through ET and latent heat LE such that the latent heat of vaporization ET λ = LE. The PT-JPL algorithm is a three source ET model where each component of ET is used to calculate the total flux:

$$LE = LE_I + LE_T + LE_S \tag{2}$$

where LE_I is evaporation from plant intercepted water, LE_T is transpiration from vegetation, and LE_S is soil evaporation. Ecophysiological *f-functions*, scalars between 0 and 1, limit each component from the potential rate.

Canopy interception is computed as:

$$LE_I = f_{WET}\,\alpha \frac{\Delta}{(\Delta + \gamma)} R_N{}^C \tag{3}$$

where f_{WET} is the fraction of saturated soil computed as $f_{WET} = RH^4$, where RH is the relative humidity of air, $R_N{}^C$ is the canopy net radiation calculated as $R_N{}^C = R_N - R_N{}^S$. $R_N{}^S$ is the net radiation at the soil surface

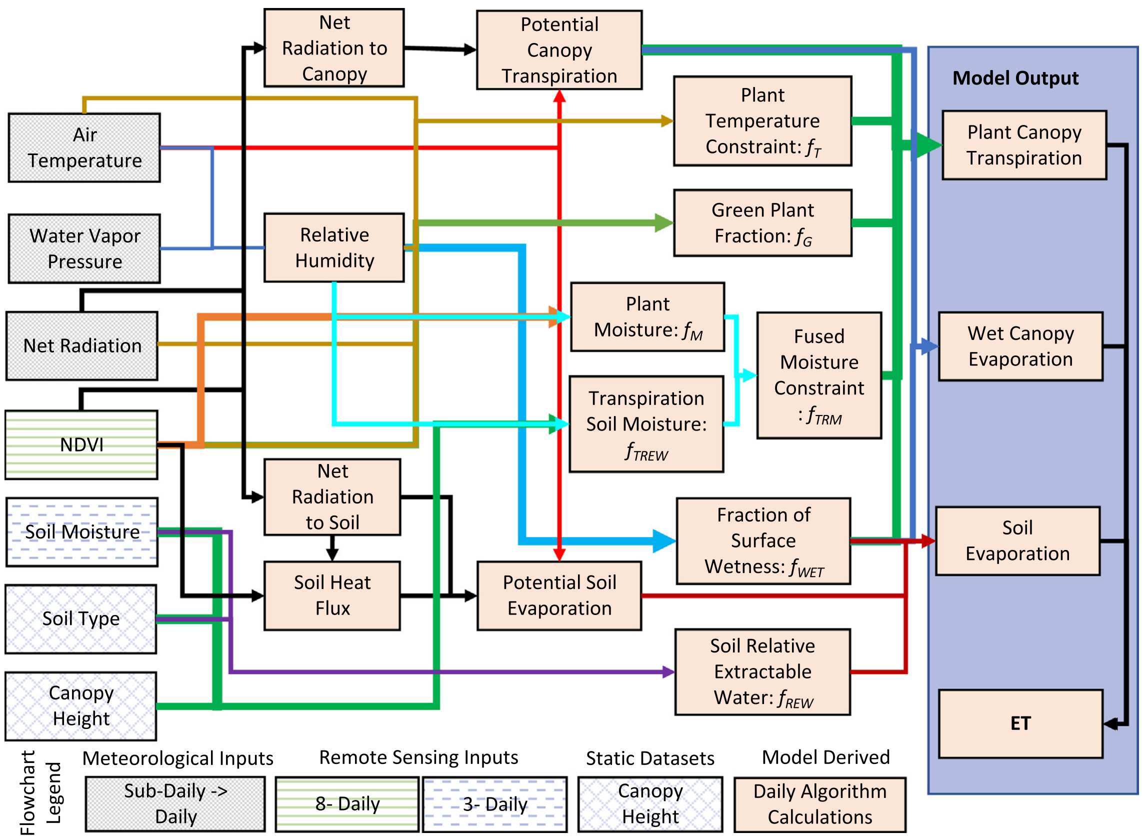

Fig. 1. Flow chart showing data processing stream for the PT-JPL$_{SM}$ model.

computed as $R_N{}^S = R_N e^{(-k_{R_n} LAI)}$ where $k_{R_n} = 0.60$ and LAI is the leaf area index.

Canopy transpiration is computed as:

$$LE_T = (1 - f_{WET}) f_G f_T f_M \alpha \frac{\Delta}{(\Delta + \gamma)} R_N{}^C \tag{4}$$

where f_G is the fractional canopy greenness computed as $f_G = \frac{f_{APAR}}{f_{IPAR}}$ where f_{APAR} is the fraction of absorbed photosynthetically active radiation (PAR) and f_{IPAR} is the fraction of intercepted PAR; f_T is the sub-optimal temperature constraint computed as $f_T = e^{\left(-\left(\frac{T-Topt}{Topt}\right)^2\right)}$ where T is the maximum daily air temperature and T_{OPT} is the optimum temperature computed as $T_{opt} = T_{\max}$ at $\max\left\{\frac{PAR f_{APAR} T_{\max}}{VPD}\right\}$ which computes when maximum plant activity is likely to occur; and f_M is the vegetation moisture constraint computed as $f_M = \frac{f_{APAR}}{f_{APAR\max}}$ where $f_{APAR\max}$ is the annual maximum f_{APAR}.

Soil evaporation is computed as:

$$LE_S = [f_{WET} + f_{SM}(1 - f_{WET})] \alpha \frac{\Delta}{(\Delta + \gamma)} (R_N{}^s - G) \tag{5}$$

where f_{SM} is the soil moisture constraint computed as $f_{SM} = RH^{VPD}$, VPD is the vapor pressure deficit. For further detail reference Fisher et al., 2008.

Soil water control on evaporation is implicitly represented through $f_{SM} = RH^{VPD}$, where f_{SM} is the soil moisture constraint on E_S, RH is the relative humidity, and VPD is the vapor pressure deficit. This equation is formed from Bouchet's theory of land atmosphere equilibrium. However, the assumption that land and atmosphere are in equilibrium at the fine spatial resolutions and acute temporal scales fails for certain regions. Similarly, plant water availability is implicitly represented by observations based on plant greenness and therefore phenological changes from peak greenness potentially introduces latent vegetation response to water limitations and overestimates transpiration.

2.2. Updates to the PT-JPL model

We update the original model, here-after called PT-JPL$_{SM}$, to incorporate explicit soil water availability control on evaporation and transpiration. Because we now model ET at sub-monthly time scales, we also integrate a new G parameterization.

Table 1
Global gridded forcing dataset characteristics.

Variable	Product name	Time available	Frequency	Spatial resolution	Reference
Net radiation	MERRA2 M2T1NXLND	1979–present	Hourly	0.5° × 0.5°	GMAO, 2015a
Temperature	MERRA2 M2I1NXASM	1979–present	Hourly	0.5° × 0.5°	GMAO, 2015b
Vapor pressure	MERRA2 M2I1NXASM	1979–present	Hourly	0.5° × 0.5°	GMAO, 2015b
NDVI	MOD13A2 MYD13A2	2000–present	8-daily	5 km × 5 km	Didan 2015a, 2015b
Soil moisture	SPL3SMP_E v1 SPL3SMP v4	4-2015–present	3-daily	9 km × 9 km	O'Neill et al., 2016
				36 km × 36 km	O'Neill et al., 2016
Soil properties	SPL4SMLM	NA	NA	9 km × 9 km	Das, 2013
Canopy height	NA	NA	NA	1 km × 1 km	Simard et al., 2011

2.2.1. Soil moisture control on evaporation

Surface soil moisture and soil properties control the rate of evaporation. As such we employ the available water content to scale the rate of evaporation. The relative extractable water is a commonly used stressor that normalizes the impact from soil properties. The original model employs the f_{SM} scalar to limit the rate of evaporation from the soil surface. This scalar was formulated to represent relative extractable water through the Bouchet's theory of where the land surface and near surface atmosphere are in equilibrium across certain space and time scales. Here we update the model to represent true relative extractable water using:

$$f_{REW} = \frac{\theta_{obs} - \theta_{wp}}{\theta_{FC} - \theta_{wp}} \tag{6}$$

where θ_{obs} is the soil moisture observation, θ_{WP} is the soil-plant wilting point, and θ_{FC} is the soil field capacity. We replace f_{SM} with f_{REW} in the new evaporation algorithms.

$$LE_S = [f_{WET} + f_{REW}(1 - f_{WET})]\alpha\frac{\Delta}{(\Delta + \gamma)}(R_N{}^s - G) \tag{7}$$

This method has been implemented in other remote sensing ET algorithms that use ET to model surface and root zone soil moisture (Anderson et al., 2007; Martens et al., 2017).

2.2.2. Soil moisture control on transpiration

In the original PT-JPL formulation plant moisture stress is inferred from the deviation from maximum greenness (f_M). As the model was originally developed for application at monthly or longer timescales, the latent responses from vegetation to moisture deficits did not impact quantification of ET, as it does at higher temporal frequencies, *i.e.* daily calculations. Therefore, we formulate and include a new soil water availability constraint on transpiration. Since shorter vegetation responds more quickly than compared to taller vegetation to precipitation deficits, above ground observations may provide insight into plant resiliency to a limited moisture supply (Knoop and Walker, 1985). Plant access to deeper water has been shown to increase resilience and survival probability to prolonged drought (Canadell et al., 1996; Giardina et al., 2017; Nepstad et al., 1994; Padilla and Pugnaire, 2007). Unfortunately, the science communities understanding of rooting depth, density and access to the water table has limited previous attempts to implement soil moisture limitations within ET models (Kelliher et al., 1993). Therefore, we implicitly represent plant resilience to soil water deficits through above ground satellite observable canopy characteristics. Previous studies have applied canopy characteristics to infer sensitivity to soil water availability (Dewaele et al., 2017; Martens et al., 2017). We acknowledge at aggregated scales a robust direct relationship between above ground biomass or canopy and resilience to drought depends on other factors such as functional rooting depth, species composition, water table depth, geology, and plant age (Fan et al., 2017; Giardina et al., 2017). However, for the purposes of this study, we apply canopy height as one variable to infer plant sensitivity to surface soil water availability. We posit that canopy height is related to the rooting depth and potential to access water from deeper sources. Therefore, canopy height data facilitate a continuous quantification of plant sensitivity to surface soil water conditions (Canadell et al., 1996; Jackson et al., 1999; Martens et al., 2017; Nepstad et al., 1994). We calculate the new transpiration constraint as:

$$f_{TREW} = 1 - \left(\frac{\theta_{CR} - \theta_{obs}}{\theta_{CR} - \theta_{wp_{CH}}}\right)^{CH_{scalar}} \tag{8}$$

where θ_{CR} is the critical soil moisture at which soil water availability limits ET, $CH_{scalar} = \sqrt{CH}$ is a canopy height (CH) scalar that impacts the sensitivity to soil water availability, set to range from 1 to 5.

$$\theta_{CR} = (1 - p)(\theta_{FC} - \theta_{wp_{CH}}) + \theta_{wp_{CH}} \tag{9}$$

$$p = \frac{1}{1 + PET} - a\frac{1}{1 + CH} \tag{10}$$

$$\theta_{WP_{CH}} = \frac{\theta_{WP}}{CH_{scalar}} \tag{11}$$

$$f_{TRM} = (1 - RH^{4(1-VWC)(1-RH)})f_M + (RH^{4(1-VWC)(1-RH)})f_{TREW} \tag{12}$$

where p is a parameter dependent on both PET [mm/day] and CH [m] that quantifies at which point soil water availability begins to limit transpiration below the potential rate, a is a parameter set to 0.1 represents the weight of influence CH imposes on θ_{CR}, and $\theta_{wp_{CH}}$ is the canopy height adjusted surface soil moisture wilting point. Eq. (8) was formed from the influence of Martens et al. (2017), but adjusted to incorporate the atmospheric demand and canopy height as continuous scalars to avoid dependence on land classification datasets. Eqs. (9) and (10) were amended from van Diepen et al. (1989), to account for the influences of plant access to deeper water reserves and atmospheric demand intensifying or mitigating vegetation sensitivity to water availability(van Diepen et al., 1989). The shape of this response curve illustrates how canopy height, the potential ET rate, and soil water availability impact the transpiration rate [Fig. S2]. Additionally, we apply a weighting scheme using 30-day mean relative humidity and soil moisture to determine when f_M or f_{TREW} are the dominant control on transpiration globally [Fig. S3]. This approach conserves the intent of the original model while leveraging the strength of soil moisture information. By weighting the influence of each scalar, we maintain or improve transpiration estimates across dry and wet ecohydrological regimes. The parameters in Eqs. (8), (9), (10), (11), and (12) were not optimized to the evaluation dataset to maintain model ability to represent ET and soil water limiting conditions globally. The new ecophysiological scalar f_{TRM} in Eq. (12) is combined in series with the combined stresses from f_G and f_T.

$$LE_T = (1 - f_{WET})f_{TRM}f_Gf_T\alpha\frac{\Delta}{(\Delta + \gamma)}R_N{}^C \tag{13}$$

2.2.3. Ground heat flux

Previously, since PT-JPL was implemented at monthly time resolution G was estimated to be 0. For daily ET calculation, we derive G as described in Allen et al. (2007), but update the parameterizations based on tall and short canopies. The updated model parameters were calibrated to a G evaluation dataset (Purdy, 2018; Purdy et al., 2016). Both PT-JPL and PT-JPL$_{SM}$ are updated to include G. The equations used to model G and the updated parameterizations are presented in the supplemental material.

3. Datasets and data processing

3.1. Global and in situ model forcing datasets

We combine satellite observations of vegetation and surface soil moisture with meteorological data from a reanalysis dataset to model ET globally. We evaluate the model using both *in situ* and gridded forcing datasets. *In situ* meteorological (R_{NET}, T_{AIR}, e_A), soil moisture (θ), and latent heat observations at integrated spatial scales from these two networks facilitate updates to the PT-JPL algorithm. Gridded forcing data from MERRA, the MODerate resolution Imaging Spectrometer (MODIS), ICESat/GLAS, and SMAP provide spatially continuous data sources to model ET globally. All datasets are open access and available from: the NASA Land Process Distributed Archive Center (https://e4ftl01.cr.usgs.gov/; http://daac.ornl.gov/MODIS/), the Goddard Earth Sciences Data and Information Services Center (https://goldsmr4.gesdisc.eosdis.nasa.gov:443), the National Snow and Ice Data Center (https://n5eil01u.ecs.nsidc.org), the COsmic-ray Soil Moisture Observing System (COSMOS) (http://cosmos.hwr.arizona.edu), the Lawrence Berkley Livermore National Laboratory's Ameriflux

Table 2
Eddy covariance tower characteristics. COSMOS soil moisture observations are taken at or near each of the towers used for *in situ* forcing evaluation or both. The towers used for gridded forcing evaluation contain data after 4/2015 and are ordered based on the aridity index calculated as annual potential evapotranspiration divided by precipitation.

Site	Latitude (°N)	Longitude (°W)	PFT	Time span	Precip (mm)	Temp (°C)	Elevation (m)	Aridity index	Tower use	PI/citation
US-SCs	33.734	−117.696	OSH	2011–2012	375.44	18.545	475	3.29	*In situ*	Goulden, 2017
US-Whs	31.743	−110.052	OSH	2015	338.54	17.135	1370	3.08	Grid	Scott, 2017a
US-SCg	33.737	−117.695	GRA	2012–2015	378.83	18.565	470	2.81	*In situ*	Goulden, 2017
US-SRM	31.821	−110.866	WSA	2015	409.04	18.445	1120	2.71	Grid	Scott, 2017b
US-Wkg	31.736	−109.941	GRA	2012–2015	380.01	16.51	1531	2.43	Both	Scott, 2017c
US-SCc	33.610	−116.450	OSH	2012–2014	371.39	15.045	1280	2.18	*In situ*	Goulden, 2017
US-Ton	38.431	−120.966	WSA	2015	610.68	16.39	177	1.95	Both	Baldocchi, 2017a
US-SRG	31.789	−110.828	GRA	2015	513.79	17.935	1291	1.87	Grid	Scott, 2017d
US-Var	38.407	−120.951	GRA	2015	608.35	16.4	129	1.86	Grid	Baldocchi, 2017b
US-Me2	44.452	−121.557	ENF	2012–2014	555	7.215	1253	1.54	*In situ*	Law, 2017
US-CZ2	37.031	−119.256	MF	2012–2015	883.31	13.785	1160	1.29	*In situ*	Goulden, 2017
US-UMB	45.559	−84.713	DBF	2012–2014	770.29	6.01	234	0.95	*In situ*	Gough et al., 2017
US-MOz	38.744	−92.200	DBF	2013–2015	1089.87	12.8	219.4	0.88	Both	Wood & Gu, 2017
US-MMS	39.323	−86.413	DBF	2012–2013	1148.53	12.02	275	0.83	*In situ*	Novick & Phillips, 2017
US-CZ3	37.067	−119.195	ENF	2012–2015	1033.73	9.225	2014	0.82	*In situ*	Goulden, 2017
US-Ro1	44.714	−93.089	CRO	2012	823.02	7.535	260	0.81	*In situ*	Baker et al., 2017
US-PFa	45.945	−90.2723	MF	2015	823	4.33	470	0.77	Grid	Desai, 2017
US-Ho1	45.204	−68.740	ENF	2012–2013	1143.42	5.84	60	0.63	*In situ*	Hollinger, 2017
US-GLE	41.364	−106.239	ENF	2012–2013	953.06	0.245	3197	0.59	*In situ*	Massman, 2017

repository (http://ameriflux.lbl.gov) and the FLUXNET data center (http://fluxnet.fluxdata.org). Table 1 describes the spatial extent and frequency characteristics of each dataset used in this study. Table 2 details the eddy covariance towers from Ameriflux used in this analysis including site locations, plant functional types, and climate and terrain sampled for the areas used to support this analysis.

3.1.1. *Modis NDVI (MOD13A2 & MYD13A2)*

The normalized difference vegetation index (NDVI) facilitates monitoring vegetation green up and senescence. The MOD13C21 and MYD13C1 data products from MODIS, when combined, provide NDVI observations at 8-day and 0.05° from the Terra and Aqua satellites from 2000 to present for global estimates (Didan, 2015a; Didan, 2015b). For *in situ* model runs, we use the Oak Ridge National Laboratory MODIS land product subset tool to extract higher spatial resolution (250 m) NDVI observations from MOD13A1 and MYD13A1 for each eddy covariance tower location, or tower principal investigator suggested representative pixel (http://daac.ornl.gov/MODIS/). All NDVI data are filtered for only high-quality observations and linearly interpolated for daily application.

3.1.2. *Canopy height (ICESat/GLAS)*

Global observations of canopy height (1-km^2) are used to model plant sensitivity to surface soil moisture. This canopy height dataset was generated with observations spanning 2003 to 2009 from the Geoscience Laser Altimeter System (GLAS) on the Ice, Cloud, and land Elevation Satellite (Simard et al., 2011). We spatially average this dataset to each of the EASE grids used in this study to model vegetation sensitivity to surface soil moisture.

3.1.3. *SMAP surface soil moisture (SPL3SMP & SPL3SMP_E)*

We use two SMAP soil moisture data products: SMAP_L3_SM_P and SMAP_L3_SM_P_E. The SMAP Level 3 Radiometer Global Daily 36 km EASE-Grid Soil Moisture Version 4 and the SMAP Enhanced Level 3 Radiometer Global Daily 9 km EASE-Grid Soil Moisture Version 1 datasets were used to compare with *in situ* observations and model ET globally for this study (O'Neill et al., 2016a; O'Neill et al., 2016b). Each dataset provides global coverage every 3 days. The SMAP mission leveraged lessons from previous soil moisture observing satellites such as the Soil Moisture and Ocean Salinity (SMOS) to incorporate radio frequency interference detection and mitigation to provide more continuous high quality global coverage of soil moisture (Mohammed et al., 2016; Oliva et al., 2012).

Soil moisture data are filtered for high-quality data which prevents using SMAP observations in urban areas, areas with high fractions of surface water, areas impacted by radio frequencies in the same microwave wavelengths as SMAP, and densely forested or highly productive agricultural regions where vegetation water content is high. The densely forested and agriculture regions that have high vegetation water content suffer from degraded surface soil moisture retrieval accuracy from space. However, many of these areas exist in regions with abundant water availability and high humidity, which mitigates potential issues of data value for ET modeling globally.

3.1.4. *Soil properties*

The soil properties used in this study are from the SMAP L4RZ dataset and sourced from the Harmonized World Soil Database version 1.2.1 (HWSD1.21) and the State Soil Geographic project (STATSGO2). These data have been re-gridded to the EASE-2 grid to maintain consistency with the SMAP Level 2 retrieval algorithms (Das et al., 2013). For the 36-km runs, we use the nested mean of the 9-km soil properties. Soil properties extracted from this dataset include the porosity and the wilting point.

3.1.5. *MERRA2: net radiation, temperature, vapor pressure*

Net radiation, air temperature, and vapor pressure data from MERRA2 reanalysis datasets M2T1NXLND and M2T1NXASM were used in this study. The MERRA2 reanalysis data provides 3-hourly data at a 0.5° latitude × 0.625° longitude global grid. We take a daily average air temperature, water vapor pressure, and net radiation, daytime maximum temperature and net radiation, and daytime minimum water vapor pressure and resample these data to the EASE grid resolutions (9-km and 36-km) to complete this study. Resampling meteorological data to finer spatial resolutions introduces uncertainty but is required due to the lack of continuous global datasets. Global ET quantification continues to rely on continuous forcing datasets from reanalysis datasets (Anderson et al., 2011; Martens et al., 2017; Mu et al., 2011). Therefore, the quality of the computed ET ultimately is dependent on the accuracy of each reanalysis variable and the subsequent potential biases including the density of observation networks in North America and Europe (Badgley et al., 2015).

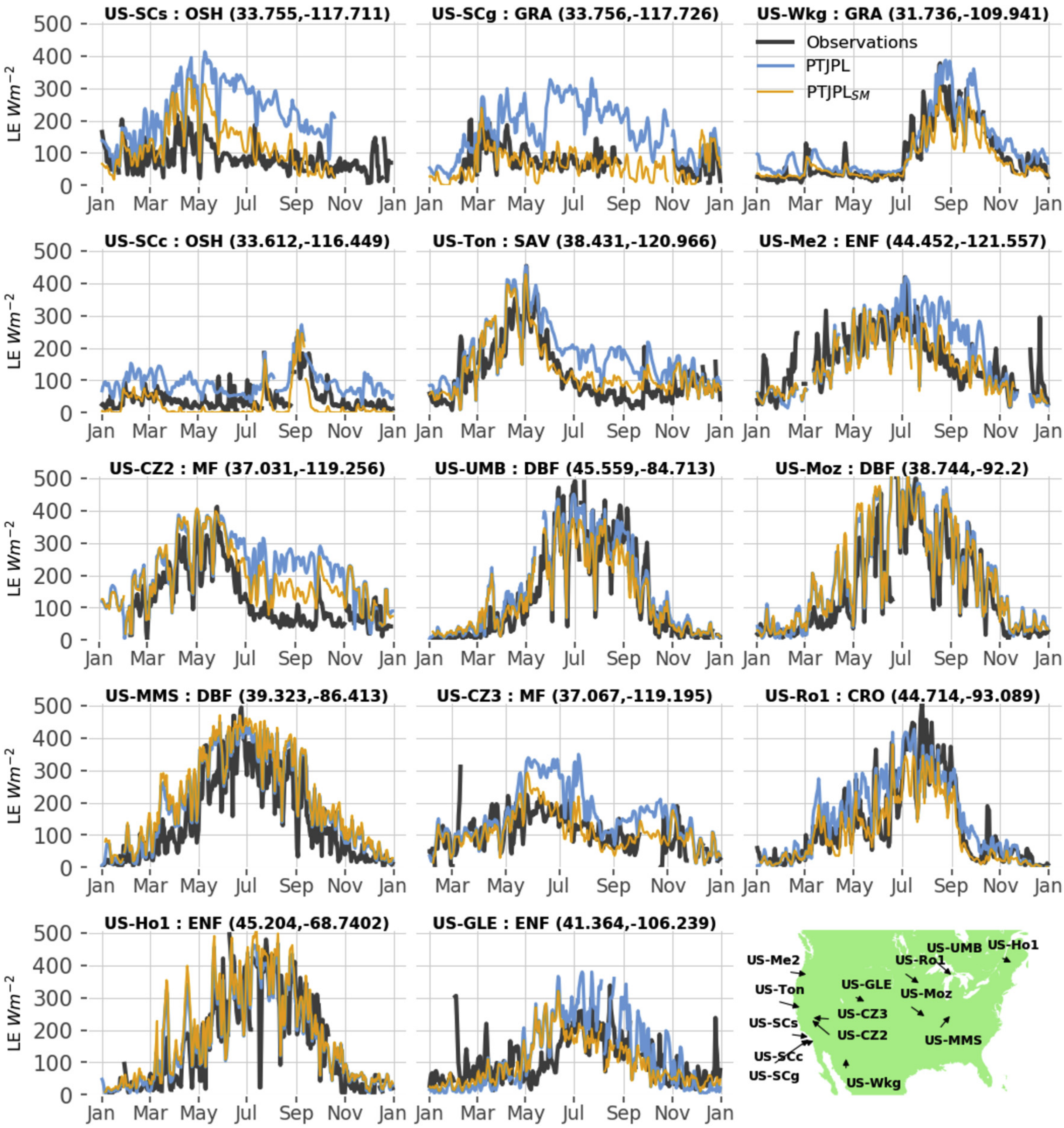

Fig. 2. *In situ* model performance across 14 Ameriflux eddy covariance sites distributed across the US. The PT-JPL$_{SM}$ model is shown with orange and the original model is shown in blue. Sites are ordered based on their aridity index from top (more dry) to bottom (more wet) [Table 2]. PT-JPL$_{SM}$ better estimates ET at more arid locations compared to PT-JPL [Table 3].

3.2. Ameriflux and COSMOS: in situ evaluation datasets

Eddy covariance observations of LE with coincident integrated measures of soil moisture are used for model evaluation [Table 2]. Many EC towers that are part of these networks measure soil moisture with 1 to 4 dielectric sensors. With limited observations, the inherent variability in soil moisture adds observational uncertainty with potential to confound model formulation and parameterizations (Ryu and Famiglietti, 2005). Soil moisture variability increases with spatial extent and during the transition from saturated to dry conditions, conditions critical for the success of modeling soil water control on ET (Famiglietti et al., 2008). The COsmic-ray Soil Moisture Observing System (COSMOS) overcomes issues of spatial representativeness by using observations of cosxmic-ray neutrons to measure soil moisture at integrated scales similar to the footprints of ET measurements from EC towers (Köhli et al., 2015; Zreda et al., 2012, 2008). Additionally, these observations have been used to validate SMAP observations within expected mission error limits (Montzka et al., 2017). Coincident integrated observations of soil moisture, ET, and meteorological data from EC towers facilitates model updates and evaluation.

We use observations from 14 EC sites that cover 7 plant functional types and varying climatic conditions. Half of the 14 sites are classified as water limited based on the Budyko Classification where the aridity index, calculated as the mean annual potential evapotranspiration divided by the mean annual precipitation, is > 1. We supplement the meteorological observations of FLUXNET and soil moisture observations from COSMOS with satellite observations of vegetation characteristics. Vegetation observations of CH and NDVI are extracted from satellite sources at 1-km resolution (http://daac.ornl.gov/MODIS/).

Table 2 provides the site locations, plant functional types, terrain, and climate sampled of the locations. We indicate whether the site was used to evaluate model updates using *in situ* evaluation, gridded forcing variables, or both *in situ* and gridded forcing variables. *In situ* LE evaluations were only performed for sites with high quality meteorology, soil moisture, and LE observations with at least 1 year of data. Gridded forcing assessments were performed for sites with LE observations since

Table 3
PT-JPL and PT-JPL$_{SM}$ performance as indicated by BIAS, RMSE, and R^2.

Site	PT-JPL			PT-JPL$_{SM}$		
	BIAS	RMSE	R^2	BIAS	RMSE	R^2
US-SCs	137.8	145.10	0.37	51.9	60.90	0.64
US-SCg	105.5	137.90	0.01	4.6	38.40	0.36
US-Wkg	21.4	27.60	0.94	6.9	24.30	0.96
US-SCc	54.0	56.30	0.76	16.2	21.60	0.78
US-Ton	67.3	75.90	0.79	20.0	33.20	0.88
US-Me2	21.1	65.20	0.65	6.4	33.40	0.82
US-CZ2	87.9	106.60	0.63	60.7	74.90	0.79
US-UMB	29.4	50.30	0.90	19.3	54.50	0.85
US-Moz	43.3	49.40	0.97	41.8	48.60	0.97
US-MMS	52.5	57.60	0.97	65.7	70.50	0.96
US-CZ3	33.7	60.20	0.62	9.0	35.60	0.63
US-Ro1	19.1	40.00	0.90	22.4	37.10	0.96
US-Ho1	46.4	62.00	0.88	62.6	79.50	0.85
US-GLE	15.4	55.90	0.79	14.8	48.20	0.48
AI > 1	70.7	87.80	0.59	23.8	40.96	0.75
AI < 1	34.3	53.63	0.86	33.7	53.43	0.81
All sites	52.5	70.71	0.73	28.7	47.19	0.78

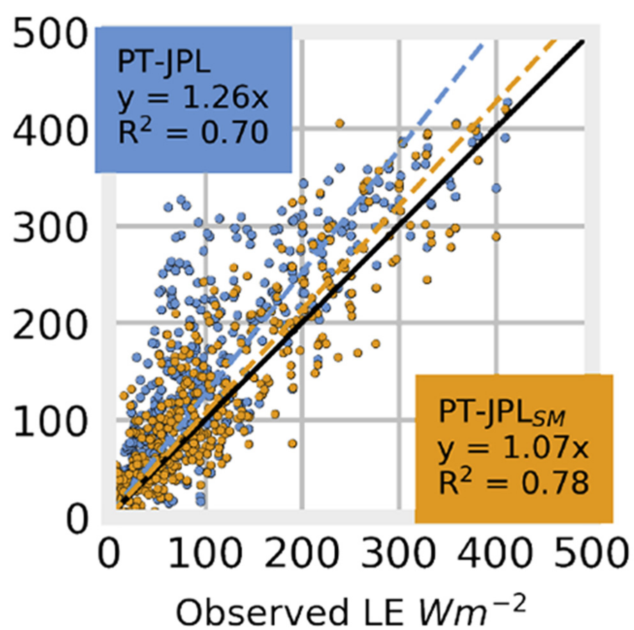

Fig. 3. Monthly scatter plot of ET model without (blue) and with (orange) soil moisture.

March 31, 2015, the start date of SMAP observations. Data availability from Ameriflux *in situ* observations during this time period and the SMAP recommended quality flag limit the number of sites used in this analysis. These constraints limited the available tower observations to 8 locations distributed across the continental United States. Numerous studies have examined the impact on eddy covariance tower footprint to gridded forcing data mismatches, but this type of analysis is outside of the scope of the current study (Amiro, 1998; Chen et al., 2009). Since eddy covariance observations of LE suffer from energy closure imbalance, we force energy balance closure daily (Foken et al., 2011; Twine et al., 2000).

4. Results

4.1. Model evaluation with in situ forcing

The *PT-JPL* and *PT-JPL$_{SM}$* models were executed daily for *in situ* evaluation and global analyses with SMAP. The *in situ* modeled LE from both PT-JPL and PT-JPL$_{SM}$ shows strong agreement with observations [Fig. 2, Table 3]. Fig. 2 compares one year of mid-day modeled LE with *in situ* observations from 14 EC towers. Sites are ordered from dry (top) to wet (bottom) based on the aridity index, a ratio of annual precipitation to PET. The PT-JPL$_{SM}$ model demonstrates greater skill than PT-JPL model at water limited sites [Table 3]. On average the PT-JPL$_{SM}$ shows a decrease in BIAS (PT-JPL: 70.7 Wm^{-2}, PT-JPL$_{SM}$: 23.8 Wm^{-2}), a large decrease in RMSE (PT-JPL: 87.8 Wm^{-2}, PT-JPL$_{SM}$: 40.9 Wm^{-2}) and an increase in explanation of variance (PT-JPL: 0.59, PT-JPL$_{SM}$: 0.75) when compared to the PT-JPL. Mean annual BIAS, RMSE, and explanation of variance improved across all water limited sites. The greatest overall statistical improvement was observed at US-SCs and US-SCg. Both of these sites have very dry conditions and a large fraction of LE comes from soil evaporation. Additionally, the years examined for these sites were part of the multi-year California drought, which exacerbated the importance of soil moisture to model LE. In addition to US-SCs and US-SCg, the largest improvements in explanation of variance occurred US-Ton, US-Me2, and US-CZ2. At the US- Ton, US-Me2, and US-CZ2 the PT-JPL$_{SM}$ model demonstrates improvements to model estimation of LE during the seasonal dry down. Lastly, at US-SCc and US-Wkg LE response to short interval precipitation events is best modeled by PT-JPL$_{SM}$ where increases and subsequent dry down of soil moisture control LE [Fig. S4].

For the mesic to wet sites (US-UMB, US-Moz, US-MMS, US-CZ3, US-Ro1, US-Ho1, US-GLE) the PT-JPL$_{SM}$ shows, on average, a small decrease in BIAS (PT-JPL: 34.3 Wm^{-2}, PT-JPL$_{SM}$: 33.7 Wm^{-2}), a small decrease in RMSE (PT-JPL: 53.6 Wm^{-2}, PT-JPL$_{SM}$: 53.4 Wm^{-2}), and a small decrease in explanation of variance (PT-JPL: 0.86, PT-JPL$_{SM}$ 0.81) when compared to PT-JPL. For very wet regions, we posit transpiration from vegetation at these EC tower locations is more sensitive to atmospheric conditions and phenological changes than fluctuations in surface soil water availability. For these locations, the model weighting scheme places more importance on f_M as a control on transpiration. The PT-JPL$_{SM}$ model shows reduced errors at US-CZ3 with soil moisture limitations. This site was in the midst of a multi-year drought with the forest moving towards water-limiting conditions providing support for use of soil moisture for water limiting regimes. For wet forested sites (US-MMS and US-Ho1), we find changes to the model resulted in an increase in error for mid-day LE estimates. However, the increased errors (15% and 10% LE) still fall within mid-day LE observational uncertainty for these sites (Hollinger and Richardson, 2005; Oliphant et al., 2004). The results from these sites demonstrate soil moisture has no added value in areas of high soil water availability. Overall, the new algorithm results in an improvement of model skill for mesic to wet sites.

We find site-wide average improvement in BIAS, RMSE, and R^2 as a result of model improvements. Additionally, incorporating explicit soil moisture improved estimates of mean monthly LE [Fig. 3]. The PT-JPL$_{SM}$ model shows greater explanation of variance (PT-JPL: 0.70, PT-JPL$_{SM}$: 0.78) and a slope (PT-JPL: 1.26, PT-JPL$_{SM}$: 1.07) closer to 1.0 compared to the PT-JPL model. Observations between 0 and 150 Wm^{-2} are better represented by the new model with a scatter closer to the 1:1 line from reduced overestimation in LE. Since the algorithm models each component separately, we quantify the added value from incorporating soil moisture into soil evaporation and canopy transpiration separately. We find by only replacing LE_S, BIAS is reduced by 30%, RMSE is reduced by 23%, and explanation of variance improves by 4.7%. By only replacing LE_T, BIAS is reduced by 30%, RMSE is reduced by 17%, and explanation of variance is reduced by 0.9%. The results of modeling LE using *in situ* forcing data demonstrates value in surface soil moisture observations for modeling ET. Next, we evaluate PT-JPL$_{SM}$ with gridded meteorology and surface soil moisture observations from SMAP with *in situ* LE observations and compared to the original model.

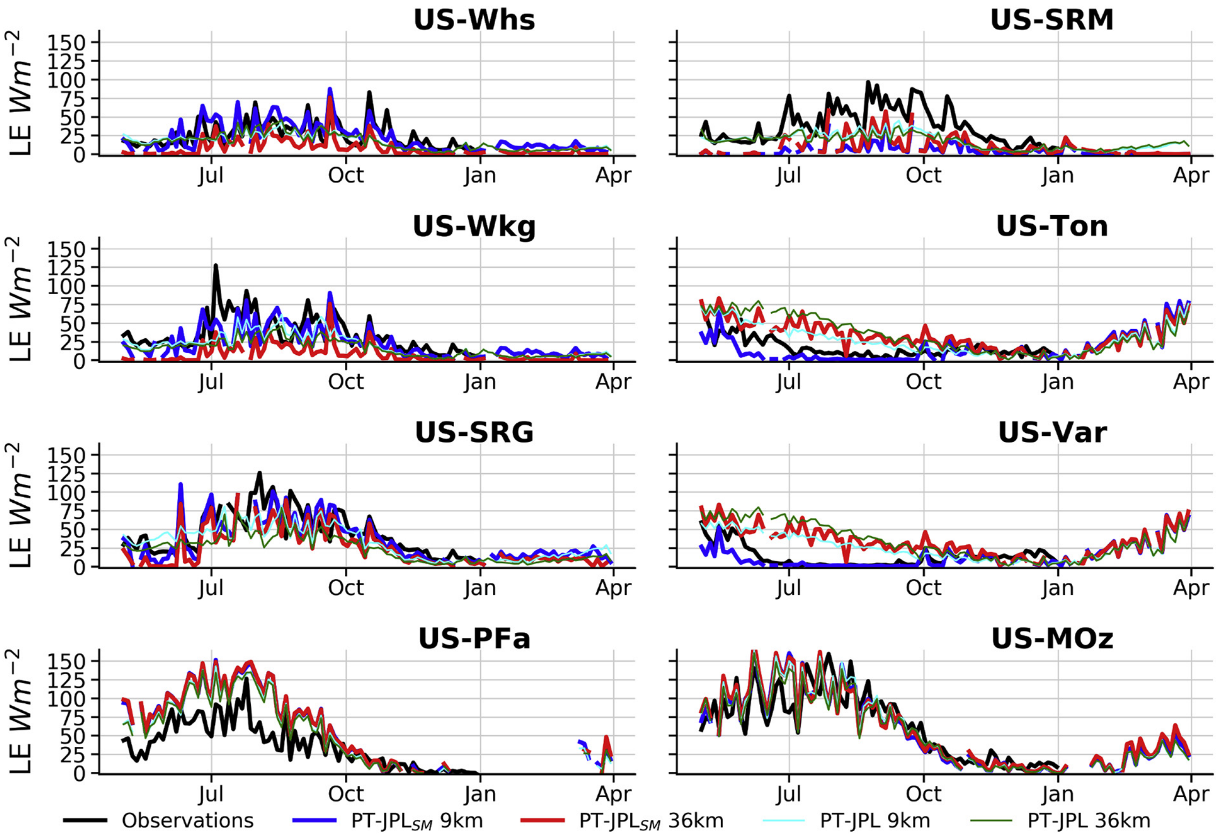

Fig. 4. Model evaluation at 6 Ameriflux EC towers with gridded forcing data. A 3-day moving average is applied to all datasets. Observations are shown in black, ET modeled with PT-JPL$_{SM}$ using SMAP_L3_P_E shown in blue, and PT-JPL$_{SM}$ using SMAP_L3_P shown in red. The PT-JPL model is shown in cyan (9-km) and green (36-km).

Table 4
PT-JPL and PT-JPLSM model performance evaluation for both 9 km and 36 km resolutions compared with 8 sites from Fig. 4.

Site	9 km				36 km			
	PT-JPL		PT-JPL$_{SM}$		PT-JPL		PT-JPL$_{SM}$	
	RMSE	R^2	RMSE	R^2	RMSE	R^2	RMSE	R^2
US-Whs	15.1	0.16	12.4	0.38	15.0	0.17	20.2	0.37
US-SRM	25.4	0.34	33.9	0.39	27.1	0.39	27.7	0.44
US-Wkg	21.7	0.29	20.6	0.43	25.0	0.26	32.1	0.33
US-Ton	17.7	0.36	14.2	0.29	29.8	0.18	19.3	0.19
US-SRG	22.2	0.40	20.9	0.58	28.7	0.36	26.2	0.57
US-Var	21.8	0.11	11.9	0.48	34.7	0.03	21.9	0.18
US-Pfa	32.9	0.51	38.8	0.51	32.0	0.52	39.4	0.52
US-MOz	22.4	0.75	23.4	0.73	22.1	0.73	23.7	0.72
All site mean	22.4	0.36	22.0	0.47	26.8	0.33	26.3	0.41

4.2. Model evaluation of global PT-JPL$_{SM}$ using SMAP soil moisture

The PT-JPL and PT-JPL$_{SM}$ algorithms were successfully applied globally using the SMAP SM_L3_P and SM_L3_P_E data. We only evaluate the gridded PT-JPL and PT-JPL$_{SM}$ for times when SMAP observations are available (*e.g.* we mask out days in PT-JPL for when SMAP data do not exist). We avoid temporal interpolation in the evaluation to prevent erroneous results. For example, interpolation during dry down events is predictable, but considerable error might be introduced interpolating before and after precipitation would lead to underestimation of total LE. Therefore we evaluate the modeled LE forced by the two SMAP soil moisture data products and at eight EC validation sites that meet SMAP QA/QC for 2015 [Table 2]. Fig. 4 compares the PT-JPL$_{SM}$ model using soil moisture from SM_L3_P (red) and SM_L3_P_E (blue) with the PT-JPL model at 9 km (cyan) and 36 km (green) and the site observations from 4/1/2015 to 12/31/2016. Both the PT-JPL$_{SM}$ and PT-JPL models capture the seasonal cycle of LE for each EC tower [Fig. 4]. Table 4 provides summary statistics for each location.

Similar to the *in situ* analysis, PT-JPL$_{SM}$ demonstrates improved seasonal dry down and response to precipitation events with both 9-km and 36-km products. For two sites that experience a Mediterranean climate (US-Ton & US-Var), where winter precipitation precedes spring warm up, PT-JPL$_{SM}$ shows an earlier decrease in modeled LE during seasonal dry downs when using SMAP data. These improvements are reflected in lower error and higher explanation of variance for PT-JPL$_{SM}$ when compared to PT-JPL at both US-Ton and US-Var [Table 4]. At US-Whs, US-Wkg, US-SRG, US-Ton, and US-Var we find PT-JPL$_{SM}$ model evaluated at 9-km shows better agreement with observations compared to the 36-km data [Table 4]. Poor model performance is observed for PT-JPL$_{SM}$ and PT-JPL at US-SRM. We posit that underestimation of modeled LE using SMAP data at the US-SRM might be due *in situ* LE observations not being representative over the heterogeneous area, a result from non-representative soil properties controlling the point at which soil moisture limits ET (*e.g.* wilting point), or an underestimation of soil moisture from SMAP. For the more humid sites, US-PFa and US-MOz, where soil water availability is non-limiting, the PT-JPL$_{SM}$ model shifts the transpiration weight towards the original model formulation which is more reliant on atmospheric conditions and phenological change. For these sites, similar to the *in situ* analysis we see similar model errors and explanation of variance for both the 9 km and 36 km results, but higher estimates of LE from the PT-JPL$_{SM}$ algorithm resulting in greater error at US-Pfa and slightly greater LE error within the range of observational uncertainty at US-MOz. Site-wide mean statistics indicate that when compared to PT-JPL, PT-JPL$_{SM}$ reduces error by 2% and 2% for both 9 km and 36 km estimates and increases explanation of

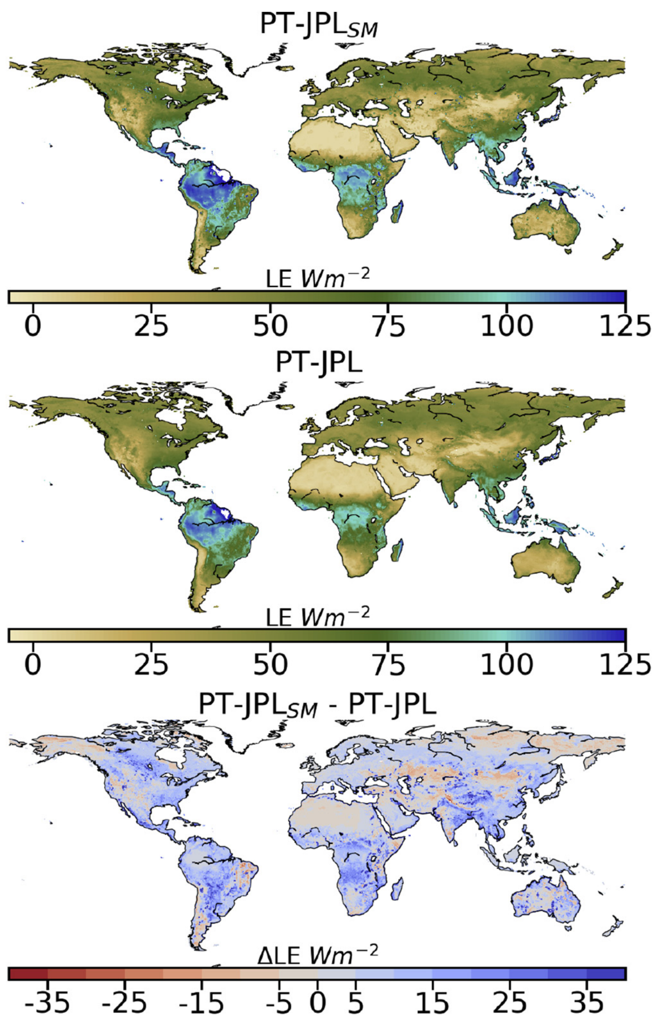

Fig. 5. Mean annual PT-JPL$_{SM}$ ET for 2016 using SMAP_L3_P_E (top), mean annual PT-JPL ET for 2016 (middle) and PT-JPL$_{SM}$-PT-JPL difference (bottom). ET data are evaluated on the 9-km EASE 2.0 Grid.

variance by 30.1% and 18.1% for the 9 km and 36 km forcing datasets respectively. Additionally, Table 4 shows PT-JPL$_{SM}$ LE modeled at 9 km results in lower error and higher explanation of variance compared to LE modeled at 36 km. Despite the soil moisture from SM_L3_P_E (9 km) being influenced by L-band microwave radiation from a larger area, the observed soil moisture data are more centered on tower locations compared to coarser the SM_L3_P (36-km) demonstrating added value for ET quantification. The limited number of validation sites prevented a robust global evaluation. Therefore, we perform a global inter-comparison between LE generated from the original PT-JPL model and new PT-JPL$_{SM}$ model. Using this analysis, we demonstrate when and where soil water-limiting conditions create the greatest disparity for global LE quantification, how soil moisture impacts LE partitioning, and how LE modeled with soil moisture impacts inter-annual variability.

4.3. Changes in global ET patterns from SMAP data

We compare the PT-JPL and PT-JPL$_{SM}$ for 2016 modeled on the 9-km grid surface. Fig. 5 shows ET from each model for 2016 and the difference between the models. Both PT-JPL and PT-JPL$_{SM}$ show expected global patterns of ET. Globally, ET is greatest in the tropics lowest at mid-latitudes. Model differences are evaluated spatially to determine where PT-JPL$_{SM}$ LE is greater than or less than the PT-JPL LE. PT-JPL$_{SM}$ modeled LE increases compared to PT-JPL in Boreal Canada, Northern and Eastern India, South America and Africa in areas surrounding the tropical belt compared to PT-JPL. These regions are dominated by transpiration and we posit that weighting moisture stress based on a 'greenness' index equally with soil moisture lessened phenological control on LE$_C$ [Fig. 5]. EC observations were not available in these regions for this study to determine if the differences result in model improvement or degradation. The largest decreases of LE from PT-JPL$_{SM}$ compared to PT-JPL occur in regions, where soil evaporation makes up the largest fraction of ET. These areas include the Southwest United States and Northern Mexico, the East Coast of Brazil, Northern Africa, Southern Africa, The Horn of Africa, western Asia and Central Australia [Fig. 5]. The largest decreases from PT-JPL$_{SM}$ occur in summer months for each respective region [Fig. S5]. These differences highlight the limited ability of f_{SM} to represent relative extractable water for daily ET modeling and highlight the value in calculating REW from using SMAP observations. Based on the results of the *in situ* evaluation and the gridded evaluation [Section 4.1], we find support that the reduced soil evaporation better reflects true ET magnitudes for these regions.

5. Discussion

5.1. Inter-annual variability of ET for 2015–2017

Global LE datasets provide a valuable tool to quantify hydrological and ecological responses to climate perturbations. We analyze inter-annual variability of LE during the peak months of the 2015–2016 El Niño intensity and compare the data to the following year [Fig. 6]. Previous studies have used LE to measure global hydrological response to El Niño. During El Niño years, global average negative LE anomalies occur relative to average LE (Miralles et al., 2014). We find that PT-JPL$_{SM}$ mean global LE for the 2015–2016 El Niño was 1.7% less than the following year. Fig. 7 shows the change in mean annual LE for both PT-JPL and PT-JPL$_{SM}$. For areas identified as having warmer or drier than average conditions during El Niño Years, such as Australia, Indonesia, Southeastern Africa, we find negative anomalies, *e.g.* lower LE when compared with the subsequent La Niña year (Vecchi and Wittenberg, 2010). In water-limited regions expected to experience more precipitation during El Niño, such as Argentina and the South West USA, we find positive LE anomalies. Similar response patterns prevail across both PT-JPL and PT-JPL$_{SM}$. However, we find subtle changes in areas such as Australia, India, and Eastern Brazil. These areas show similar signs of change, but transitional boundaries are changes which reflect changes in soil water availability. Interestingly we find increases in LE across the tropics, which contrast patterns of decreases in LE found by Miralles et al. (2014). Despite these regions experiencing decreases in precipitation, increased incoming radiation produced greater LE than the following year. As these regions are regions known as being energy-limited, contrasting LE datasets and models create an opportunity for future exploration into the controlling mechanisms of LE across these regions (Nemani et al., 2003). The PT-JPL$_{SM}$ LE data show the potential ability to distinguish explicit inter-annual changes in LE as a result of soil water limitation and serve as a tool to identify vegetation stress and drought intensity. Overall, PT-JPL$_{SM}$ demonstrates the value of using soil moisture within LE models for capturing seasonal changes, especially in drier regions where soil moisture exerts greater control on inter-annual variation.

5.2. ET partitioning

Appropriate partitioning of ET into transpiration, canopy interception, and soil evaporation is an overlooked area of ET science, yet greatly important to appropriately model these mechanistic responses to environmental conditions. Fig. 7 shows the fraction of transpiration, interception, and soil evaporation globally and each components contribution to mean annual LE. The top map illustrates the percent contribution from each component and reveals expected global patterns of

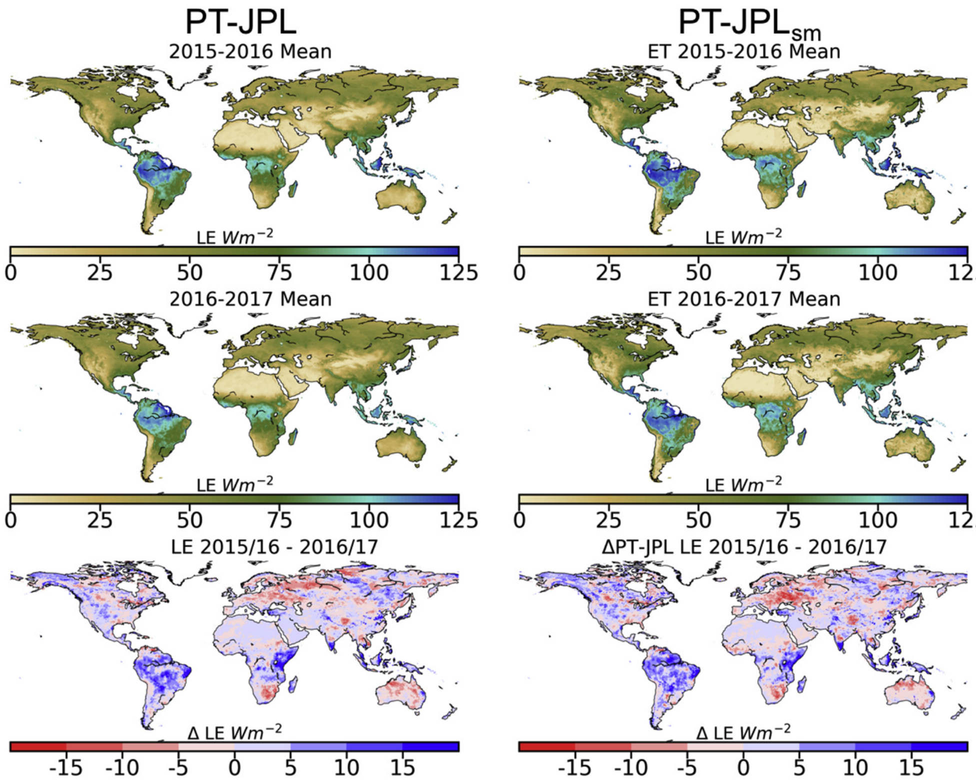

Fig. 6. Inter-annual variation in PT-JPL (left) and PT-JPL$_{SM}$ (right) LE. Top) 2015–2016 mean LE during El Niño. Middle) 2016–2017 mean LE. Bottom) Difference in LE.

dominant ET components (*e.g.* soil evaporation is greatest in deserts, transpiration is dominant in forested regions, and interception is a large fraction in rainforests). Previous ET model partitioning estimates estimate transpiration to be between 25% and 65% (Wang and Dickinson, 2012) and recent remote sensing algorithms estimate transpiration to be as high as 80% of ET globally (Miralles et al., 2011). We estimate soil evaporation, canopy transpiration, and evaporation from interception to be 23 ± 1.7%, 54 ± 1.6%, and 21 ± 0.8% of total ET annually respectively. The PT-JPL$_{SM}$ fraction of soil evaporation and canopy interception are greater than similarly reported fractions from GLEAM model 7–15% and 11–12% respectively (Martens et al., 2017; Miralles et al., 2011). Additionally, we calculate a lower fraction of canopy transpiration 54% compared to GLEAM (74–80%). The large disparity in soil evaporation and canopy transpiration can be traced to the radiation partitioning and the forcing datasets that influence $R_N{}^C$ and $R_N{}^S$ and the environmental stress imparted on the transpiration rate. We posit that the difference in canopy intercepted evaporation occurs as a result of the model's dependence on RH to calculate f_{WET}. Coarse resolution meteorological forcing resampled to finer spatial resolutions introduces larger fractions of wet surface area, especially in coastal and tropical regions where regions are more influenced by water vapor pressure. Despite these differences in ET partitioning, we find the global patterns to be similar. These large differences warrant further investigation into appropriate partitioning methodology across biomes and climates. More ground-based observations of each component at scales relevant for modeling and remote-sensing comparison are needed to reign in this large uncertainty.

The assumptions built into the models might over/under-estimate certain variables (*e.g.* temperature, water availability) impact on ET and each of its components. With regard to soil evaporation, we use the wilting point instead of the hygroscopic point to limit soil evaporation. By using the wilting point instead of the hygroscopic point, this might introduce a possible overestimation of soil moisture limitation on soil evaporation for clay and peat soils (*e.g.* clay and peat) where the soil water retention curve is less steep than sandy and loamy soils where the slope of the soil water retention curve is much greater (Hillel, 2013). Further in depths studies should focus on the mechanisms controlling transpiration and interception as well. Transpiration and the impact from deficits of soil water availability continues to be a great area of need for further analyses (Talsma et al., 2018). For transpiration, uncertainty of rooting depth and density limits applications of process-based modeling of water movement from soil through plants to the atmosphere (Schenk and Jackson, 2002). Balancing large scale changes with plant-specific resiliency depends on the underlying covariation in soil moisture and root distributions. Future observations of soil moisture and canopy transpiration as well as synthesized datasets offer a path towards model improvement (*e.g.* SAPFLUX, eddy covariance observations, & COSMOS) (Poyatos et al., 2016). Additionally, leveraging isotope observations may serve as a boundary to further guide development of model partitioning. Only when each component of ET partitioning is measured separately with low uncertainty will satellite-driven ET model partitioned components begin to be properly constrained.

6. Conclusion

We present an update to the widely used PT-JPL ET model to address one of the model's main gaps: the implicit representation of soil water control. We incorporate soil moisture constraints on evaporation and transpiration. *In situ* analyses demonstrate the largest improvements for ET estimates in dry regions. We apply SMAP soil moisture observations to model ET globally using PT-JPL$_{SM}$. The PT-JPL$_{SM}$ model shows improved model performance when compared to ground observations. Finer spatial resolution soil moisture observations at 9 km from the SMAP Level 3 Passive Enhanced product resulted in reduced LE error and increased explanation of variance compared LE forced with the 36 km SMAP Level 3 Passive product. The soil moisture constraint resulted in lower global estimates of evaporation and

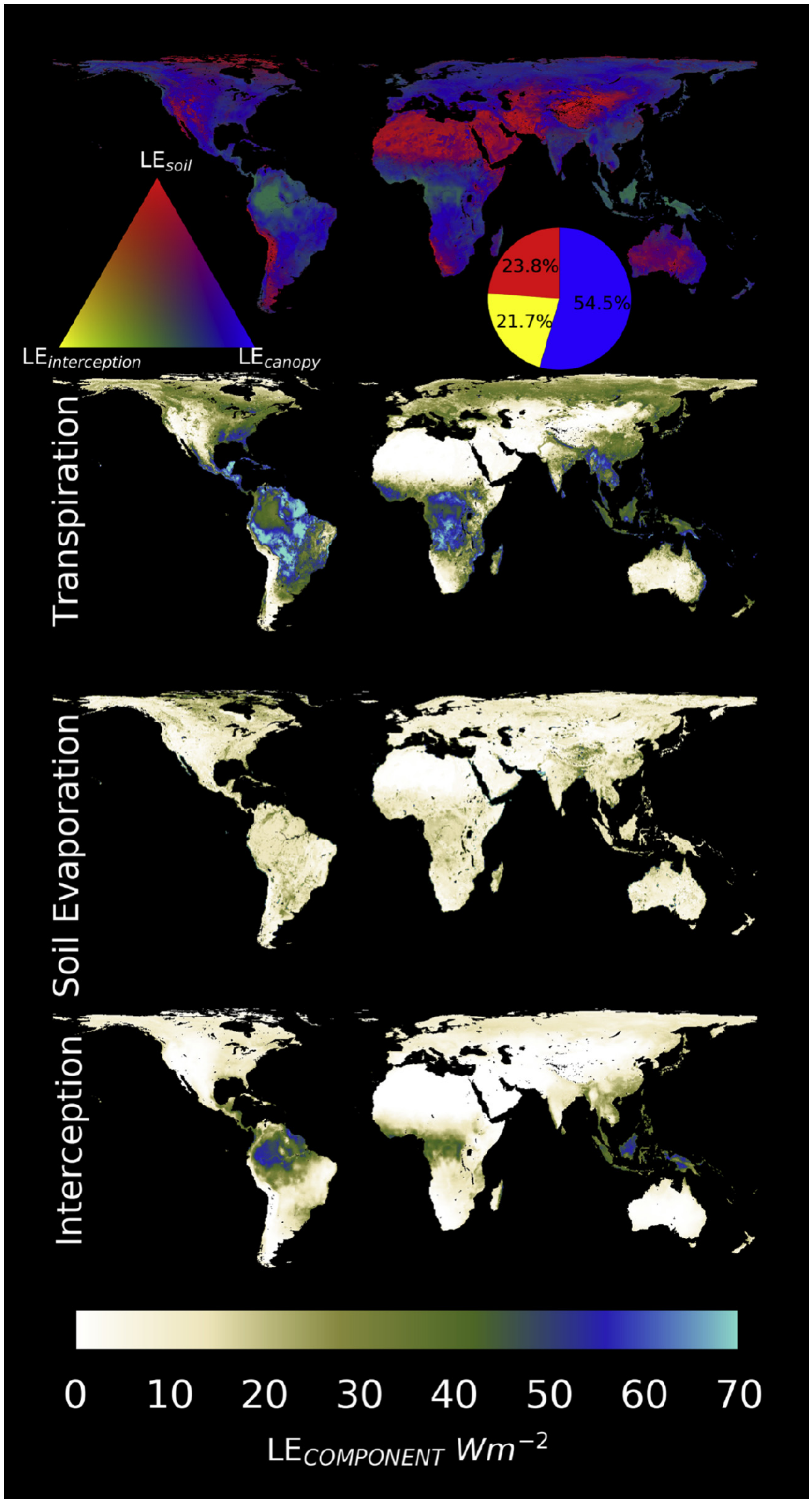

Fig. 7. Evapotranspiration components as expressed as a percentage of total ET. Red indicates more soil evaporation, blue indicates more transpiration, yellow indicates more canopy interception evaporation. Below, total contribution to annual ET from transpiration, soil evaporation, and interception.

transpiration for water-limited regions. These lower ET estimates have implications for feedbacks between the water cycle and the carbon cycle. Arid and semi-arid regions have been identified as a major contributor to the inter-annual variability in CO_2 uptake and are key areas to better understand how strong coupling between land-atmosphere moisture exchange impacts carbon uptake (Levine et al., 2016; Miralles et al., 2014, 2012; Poulter et al., 2014). The lower estimates provide a more accurate dataset to quantify water use efficiency and track impacts from drought and climate perturbations such as El Niño events. The updated PT-JPL$_{SM}$ ET model shows expected patterns of changes in ET for El-Niño and La Niña years. Based on the results in this study we conclude that modifications to the PT-JPL algorithm to include soil moisture produce more realistic ET estimates globally. This dataset provides the opportunity to identify vegetation vulnerable to drought and water limiting conditions.

Acknowledgements

AJP was supported by the NASA Earth and Space Science Fellowship 17-EARTH17R-0062 and the SUSMAP and INCA programs. JBF contributed to this research from the Jet Propulsion Laboratory, California Institute of Technology, under a contract with the National Aeronautics and Space Administration. California Institute of Technology. Government sponsorship acknowledged. JBF was supported in part by NASA's SUSMAP, INCA, IDS, GRACE, and ECOSTRESS programs. We thank an anonymous reviewer and Brecht Martens for critiques beneficial to the advancement of this manuscript.

Appendix A. Supplementary data

Supplementary data to this article can be found online at https://doi.org/10.1016/j.rse.2018.09.023.

References

Allen, R.G., Tasumi, M., Trezza, R., 2007. Satellite-Based Energy Balance for Mapping Evapotranspiration With Internalized Calibration, METRIC…— Model 380–395.

Amiro, B.D., 1998. Footprint climatologies for evapotranspiration in a boreal catchment. Agric. For. Meteorol. 90, 195–201. https://doi.org/10.1016/S0168-1923(97)00096-8.

Anderson, M.C., Norman, J.M., Mecikalski, J.R., Otkin, J.A., Kustas, W.P., 2007. A climatological study of evapotranspiration and moisture stress across the continental United States based on thermal remote sensing: 1. Model formulation. J. Geophys. Res. Atmos. 112. https://doi.org/10.1029/2006JD007506.

Anderson, R.G., Canadell, J.G., Randerson, J.T., Jackson, R.B., Hungate, B. a, Baldocchi, D.D., Ban-Weiss, G. a, Bonan, G.B., Caldeira, K., Cao, L., Diffenbaugh, N.S., Gurney, K.R., Kueppers, L.M., Law, B.E., Luyssaert, S., O'Halloran, T.L., 2011. Biophysical considerations in forestry for climate protection. Front. Ecol. Environ. 9, 174–182. https://doi.org/10.1890/090179.

Anderson, M.C., Hain, C., Otkin, J., Zhan, X., Mo, K., Svoboda, M., Wardlow, B., Pimstein, A., 2013. An intercomparison of drought indicators based on thermal remote sensing and NLDAS-2 simulations with U.S. drought monitor classifications. J. Hydrometeorol. 14, 1035–1056. https://doi.org/10.1175/JHM-D-12-0140.1.

Badgley, G., Fisher, J.B., Jiménez, C., Tu, K.P., Vinukollu, R., 2015. On uncertainty in global terrestrial evapotranspiration estimates from choice of input forcing datasets*. J. Hydrometeorol. 16, 1449–1455. https://doi.org/10.1175/JHM-D-14-0040.1.

Baker, John, Griffis, Tim, Griffis, Timothy, 2017. AmeriFlux US-Ro1 Rosemount- G21. https://doi.org/10.17190/AMF/1246092.

Baldocchi, Dennis, 2017a. AmeriFlux US-Ton Tonzi Ranch. https://doi.org/10.17190/AMF/1245971.

Baldocchi, Dennis, 2017b. AmeriFlux US-Var Vaira Ranch- Ione. https://doi.org/10.17190/AMF/1245984.

Baldocchi, D., Falge, E., Gu, L., Olson, R., Hollinger, D., Running, S., Anthoni, P., Bernhofer, C., Davis, K., Evans, R., Fuentes, J., Goldstein, A., Katul, G., Law, B., Lee, X., Malhi, Y., Meyers, T., Munger, W., Oechel, W., Paw, U.K.T., Pilegaard, K., Schmid, H.P., Valentini, R., Verma, S., Vesala, T., Wilson, K., Wofsy, S., 2001. FLUXNET: a new tool to study the temporal and spatial variability of ecosystem-scale carbon dioxide, water vapor, and energy flux densities. Bull. Am. Meteorol. Soc. 82, 2415–2434. https://doi.org/10.1175/1520-0477(2001)082<2415:FANTTS>2.3.CO;2.

Canadell, J., Jackson, R.B., Ehleringer, J.B., Mooney, H.A., Sala, O.E., Schulze, E.-D., 1996. Maximum rooting depth of vegetation types at the global scale. Oecologia 108, 583–595. https://doi.org/10.1007/BF00329030.

Chen, B., Black, T.A., Coops, N.C., Hilker, T., Trofymow, J.A., Morgenstern, K., 2009. Assessing tower flux footprint climatology and scaling between remotely sensed and eddy covariance measurements. Bound.-Layer Meteorol. 130, 137–167. https://doi.org/10.1007/s10546-008-9339-1.

Colliander, A., Cosh, M.H., Misra, S., Jackson, T.J., Crow, W.T., Chan, S., Bindlish, R., Chae, C., Holifield Collins, C., Yueh, S.H., 2017. Validation and scaling of soil moisture in a semi-arid environment: SMAP validation experiment 2015 (SMAPVEX15). Remote Sens. Environ. 196, 101–112. https://doi.org/10.1016/j.rse.2017.04.022.

Das, N., 2013. Soil Moisture Active Passive (SMAP) Ancillary Data Report Soil Attributes. SMAP science document no. 044. Jet Propulsion Laboratory. California Institute of Technology.

Desai, A., 2017. AmeriFlux US-PFa Park Falls/WLEF. https://doi.org/10.17190/AMF/1246090.

Dewaele, H., Munier, S., Albergel, C., Planque, C., Laanaia, N., Carrer, D., Calvet, J.C., 2017. Parameter optimisation for a better representation of drought by LSMs: inverse modelling vs. sequential data assimilation. Hydrol. Earth Syst. Sci. 21, 4861–4878. https://doi.org/10.5194/hess-21-4861-2017.

Didan, K., 2015a. MOD13C1 MODIS/Terra Vegetation Indices 16-Day L3 Global 0.05Deg CMG V006 [Data set]. NASA EOSDIS LP DAAChttps://doi.org/10.5067/MODIS/MOD13C1.006.

Didan, K., 2015b. MYD13C1 MODIS/Aqua Vegetation Indices 16-Day L3 Global 0.05Deg CMG V006 [Data set]. NASA EOSDIS LP DAAChttps://doi.org/10.5067/MODIS/MYD13C1.006.

Entekhabi, D., Njoku, E.G., O'Neill, P.E., Kellogg, K.H., Crow, W.T., Edelstein, W.N., Entin, J.K., Goodman, S.D., Jackson, T.J., Johnson, J., Kimball, J., Piepmeier, J.R., Koster, R.D., Martin, N., McDonald, K.C., Moghaddam, M., Moran, S., Reichle, R., Shi, J.C., Spencer, M.W., Thurman, S.W., Tsang, L., Van Zyl, J., 2010. The soil moisture active passive (SMAP) mission. Proc. IEEE 98, 704–716. https://doi.org/10.1109/JPROC.2010.2043918.

Ershadi, A., McCabe, M.F., Evans, J.P., Chaney, N.W., Wood, E.F., 2014. Multi-site evaluation of terrestrial evaporation models using FLUXNET data. Agric. For. Meteorol. 187, 46–61. https://doi.org/10.1016/j.agrformet.2013.11.008.

Famiglietti, J.S., Ryu, D., Berg, A.A., Rodell, M., Jackson, T.J., 2008. Field observations of soil moisture variability across scales. Water Resour. Res. 44. https://doi.org/10.1029/2006WR005804.

Fan, Y., Miguez-Macho, G., Jobbágy, E.G., Jackson, R.B., Otero-Casal, C., 2017. Hydrologic regulation of plant rooting depth. Proc. Natl. Acad. Sci. 201712381. https://doi.org/10.1073/pnas.1712381114.

Fisher, J.B., Tu, K.P., Baldocchi, D.D., 2008. Global estimates of the land-atmosphere water flux based on monthly AVHRR and ISLSCP-II data, validated at 16 FLUXNET sites. Remote Sens. Environ. 112, 901–919. https://doi.org/10.1016/j.rse.2007.06.025.

Fisher, J.B., Melton, F., Middleton, E., Hain, C., Anderson, M., Allen, R., McCabe, M.F., Hook, S., Baldocchi, D., Townsend, P.A., Kilic, A., Tu, K., Miralles, D.D., Perret, J., Lagouarde, J.-P., Waliser, D., Purdy, A.J., French, A., Schimel, D., Famiglietti, J.S., Stephens, G., Wood, E.F., 2017. The future of evapotranspiration: global requirements for ecosystem functioning, carbon and climate feedbacks, agricultural management, and water resources. Water Resour. Res. 53, 2618–2626. https://doi.org/10.1002/2016WR020175.

Foken, T., Aubinet, M., Finnigan, J.J., Leclerc, M.Y., Mauder, M., Paw U, K.T., 2011. Results of a panel discussion about the energy balance closure correction for trace gases. Bull. Am. Meteorol. Soc. https://doi.org/10.1175/2011BAMS3130.1.

Giardina, F., Konings, A.G., Uriarte, M., Oliveira, R.S., Gentine, P., 2017. Tall Amazonian forests are more resistant to precipitation variability. Nat. Geosci. https://doi.org/10.1038/s41561-018-0133-5. in review.

GMAO, 2015a. MERRA-2 tavg1_2d_flx_Nx: 2d, 1-hourly, time-averaged, single-level, assimilation, surface flux diagnostics V5.12.4. Goddard Earth Sciences Data and Information Services Center (GES DISC)https://doi.org/10.5067/7MCPBJ41Y0K6 , Accessed date: 1 May 2016.

GMAO, 2015b. MERRA-2 inst1_2d_lfo_Nx: 2d, 1-hourly, instantaneous, single-level, assimilation, land surface forcings v5.12.4. Goddard Earth Sciences Data and Information Services Center (GES DISC)https://doi.org/10.5067/RCMZA6TL70BG , Accessed date: 1 May 2016.

Gough, Christopher, Bohrer, Gil, Curtis, Peter, 2017. AmeriFlux US-UMB Univ. of Mich. Biological Station. https://doi.org/10.17190/AMF/1246107.

Goulden Lab, 2017. http://www.ess.uci.edu/~california.

Goulden, M.L., Bales, R.C., 2014. Mountain runoff vulnerability to increased evapotranspiration with vegetation expansion. Proc. Natl. Acad. Sci. 111, 14071–14075. https://doi.org/10.1073/pnas.1319316111.

Goulden, M.L., Anderson, R.G., Bales, R.C., Kelly, a.E., Meadows, M., Winston, G.C., 2012. Evapotranspiration along an elevation gradient in California's Sierra Nevada. J. Geophys. Res. 117, G03028. https://doi.org/10.1029/2012JG002027.

Greve, P., Seneviratne, S.I., 2015. Assessment of future changes in water availability and aridity. Geophys. Res. Lett. 42, 5493–5499. https://doi.org/10.1002/2015GL064127.

Hillel, D., 2013. Fundamentals of soil physics. In: Fundamentals of Soil Physics, https://doi.org/10.1016/C2009-0-03109-2.

Hollinger, David, 2017. AmeriFlux US-Ho1 Howland Forest (main tower). https://doi.org/10.17190/AMF/1246061.

Hollinger, D.Y., Richardson, A.D., 2005. Uncertainty in eddy covariance measurements and its application to physiological models. Tree Physiol. 873–885. https://doi.org/10.1093/treephys/25.7.873.

Huntington, T.G., 2006. Evidence for intensification of the global water cycle: Review and synthesis. J. Hydrol. https://doi.org/10.1016/j.jhydrol.2005.07.003.

Jackson, R.B., Moore, L.A., Hoffmann, W.A., Pockman, W.T., Linder, C.R., 1999. Ecosystem rooting depth determined with caves and DNA. Proc. Natl. Acad. Sci. U. S. A. 96, 11387–11392. https://doi.org/10.1073/pnas.96.20.11387.

Jarvis, P.G., Mcnaughton, K.G., 1986. Stomatal control of transpiration: scaling up from leaf to region. Adv. Ecol. Res. 15, 1–49. https://doi.org/10.1016/S0065-2504(08)60119-1.

Jin, Y., Randerson, J.T., Goulden, M.L., 2011. Continental-scale net radiation and evapotranspiration estimated using MODIS satellite observations. Remote Sens. Environ. 115, 2302–2319. https://doi.org/10.1016/j.rse.2011.04.031.

Johnson, J.T., Mohammed, P.N., Piepmeier, J.R., Bringer, A., Aksoy, M., 2016. Soil moisture active passive (SMAP) microwave radiometer radio-frequency interference (RFI) mitigation: algorithm updates and performance assessment. In: International Geoscience and Remote Sensing Symposium (IGARSS), pp. 123–124. https://doi.org/10.1109/IGARSS.2016.7729022.

Jung, M., Reichstein, M., Ciais, P., Seneviratne, S.I., Sheffield, J., Goulden, M.L., Bonan, G., Cescatti, A., Chen, J., de Jeu, R., Dolman, A.J., Eugster, W., Gerten, D., Gianelle, D., Gobron, N., Heinke, J., Kimball, J., Law, B.E., Montagnani, L., Mu, Q., Mueller, B., Oleson, K., Papale, D., Richardson, A.D., Roupsard, O., Running, S., Tomelleri, E., Viovy, N., Weber, U., Williams, C., Wood, E., Zaehle, S., Zhang, K., 2010. Recent decline in the global land evapotranspiration trend due to limited moisture supply. Nature 467, 951–954. https://doi.org/10.1038/nature09396.

Kelliher, F.M., Leuning, R., Schulze, E.D., 1993. Evaporation and canopy characteristics of coniferous forests and grasslands. Oecologia. https://doi.org/10.1007/BF00323485.

Kerr, Y.H., Al-Yaari, A., Rodriguez-Fernandez, N., Parrens, M., Molero, B., Leroux, D., Bircher, S., Mahmoodi, A., Mialon, A., Richaume, P., Delwart, S., Al Bitar, A., Pellarin, T., Bindlish, R., Jackson, T.J., Rüdiger, C., Waldteufel, P., Mecklenburg, S., Wigneron, J.P., 2016. Overview of SMOS performance in terms of global soil moisture monitoring after six years in operation. Remote Sens. Environ. 180, 40–63. https://doi.org/10.1016/j.rse.2016.02.042.

Knoop, W.T., Walker, B.H., 1985. Interactions of woody and herbaceous vegetation in a southern African savanna. J. Ecol. 73, 235–253. https://doi.org/10.2307/2259780.

Köhli, M., Schrön, M., Zreda, M., Schmidt, U., Dietrich, P., Zacharias, S., 2015. Footprint characteristics revised for field-scale soil moisture monitoring with cosmic-ray neutrons. Water Resour. Res. 51, 5772–5790. https://doi.org/10.1002/2015WR017169.

Law, Bev, 2017. AmeriFlux US-Me2 Metolius mature ponderosa pine. https://doi.org/10.17190/AMF/1246076.

Levine, P.A., Randerson, J.T., Swenson, S.C., Lawrence, D.M., 2016. Evaluating the strength of the land-atmosphere moisture feedback in earth system models using satellite observations. Hydrol. Earth Syst. Sci. 20, 4837–4856. https://doi.org/10.5194/hess-20-4837-2016.

Lo, M.H., Famiglietti, J.S., 2013. Irrigation in California's Central Valley strengthens the southwestern U.S. water cycle. Geophys. Res. Lett. 40, 301–306. https://doi.org/10.1002/grl.50108.

Martens, B., Miralles, D.G., Lievens, H., Van Der Schalie, R., De Jeu, R.A.M., Fernández-Prieto, D., Beck, H.E., Dorigo, W.A., Verhoest, N.E.C., 2017. GLEAM v3: satellite-based land evaporation and root-zone soil moisture. Geosci. Model Dev. 10, 1903–1925. https://doi.org/10.5194/gmd-10-1903-2017.

Massman, Bill, 2017. AmeriFlux US-GLE GLEES. https://doi.org/10.17190/AMF/1246056.

McDowell, N.G., 2011. Mechanisms linking drought, hydraulics, carbon metabolism, and vegetation mortality. Plant Physiol. 155, 1051–1059. https://doi.org/10.1104/pp.110.170704.

Michel, D., Jiménez, C., Miralles, D.G., Jung, M., Hirschi, M., Ershadi, A., Martens, B., Mccabe, M.F., Fisher, J.B., Mu, Q., Seneviratne, S.I., Wood, E.F., Fernández-Prieto, D., 2016. The WACMOS-ET project - part 1: tower-scale evaluation of four remote-sensing-based evapotranspiration algorithms. Hydrol. Earth Syst. Sci. 20, 803–822. https://doi.org/10.5194/hess-20-803-2016.

Miralles, D.G., De Jeu, R.A.M., Gash, J.H., Holmes, T.R.H., Dolman, A.J., 2011. Magnitude and variability of land evaporation and its components at the global scale. Hydrol. Earth Syst. Sci. 15, 967–981. https://doi.org/10.5194/hess-15-967-2011.

Miralles, D.G., Van Den Berg, M.J., Teuling, A.J., De Jeu, R.A.M., 2012. Soil moisture-temperature coupling: a multiscale observational analysis. Geophys. Res. Lett. 39. https://doi.org/10.1029/2012GL053703.

Miralles, D.G., Teuling, A.J., van Heerwaarden, C.C., Vilà-Guerau de Arellano, J., 2014. Mega-heatwave temperatures due to combined soil desiccation and atmospheric heat accumulation. Nat. Geosci. 7, 345–349. https://doi.org/10.1038/ngeo2141.

Mohammed, P.N., Aksoy, M., Piepmeier, J.R., Johnson, J.T., Bringer, A., 2016. SMAP L-band microwave radiometer: RFI mitigation prelaunch analysis and first year on-orbit observations. IEEE Trans. Geosci. Remote Sens. 54, 6035–6047. https://doi.org/10.1109/TGRS.2016.2580459.

Monteith, J.L.L., 1965. Evaporation and environment. Symp. Soc. Exp. Biol. 19, 205–234. https://doi.org/10.1613/jair.301.

Montzka, C., Bogena, H.R., Zreda, M., Monerris, A., Morrison, R., Muddu, S., Vereecken, H., 2017. Validation of spaceborne and modelled surface soil moisture products with cosmic-ray neutron probes. Remote Sens. 9. https://doi.org/10.3390/rs9020103.

Mu, Q., Zhao, M., Running, S.W., 2011. Improvements to a MODIS global terrestrial evapotranspiration algorithm. Remote Sens. Environ. 115, 1781–1800. https://doi.org/10.1016/j.rse.2011.02.019.

Mu, Q., Zhao, M., Kimball, J.S., McDowell, N.G., Running, S.W., 2013. A remotely sensed global terrestrial drought severity index. Bull. Am. Meteorol. Soc. 94, 83–98. https://doi.org/10.1175/BAMS-D-11-00213.1.

Mueller, B., Hirschi, M., Jimenez, C., Ciais, P., Dirmeyer, P.A., Dolman, A.J., Fisher, J.B., Jung, M., Ludwig, F., Maignan, F., Miralles, D.G., McCabe, M.F., Reichstein, M., Sheffield, J., Wang, K., Wood, E.F., Zhang, Y., Seneviratne, S.I., 2013. Benchmark products for land evapotranspiration: LandFlux-EVAL multi-data set synthesis. Hydrol. Earth Syst. Sci. 17, 3707–3720. https://doi.org/10.5194/hess-17-3707-2013.

Nemani, R.R., Keeling, C.D., Hashimoto, H., Jolly, W.M., Piper, S.C., Tucker, C.J., Myneni, R.B., Running, S.W., 2003. Climate-driven increases in global terrestrial net primary production from 1982 to 1999. Science 300, 1560–1563. https://doi.org/10.1126/science.1082750.

Nepstad, D.C., de Carvalho, C.R., Davidson, E.A., Jipp, P.H., Lefebvre, P.A., Negreiros, G.H., da Silva, E.D., Stone, T.A., Trumbore, S.E., Vieira, S., 1994. The role of deep roots in the hydrological and carbon cycles of Amazonian forests and pastures. Nature 372, 666–669. https://doi.org/10.1038/372666a0.

Njoku, E.G., Jackson, T.J., Lakshmi, V., Chan, T.K., Nghiem, S.V., 2003. Soil moisture retrieval from AMSR-E. IEEE Trans. Geosci. Remote Sens. 41, 215–228. https://doi.org/10.1109/TGRS.2002.808243.

Novick, Kim, Phillips, Rich, 2017. AmeriFlux US-MMS Morgan Monroe State Forest. https://doi.org/10.17190/AMF/1246080.

Novick, K.A., Ficklin, D.L., Stoy, P.C., Williams, C.A., Bohrer, G., Oishi, A.C., Papuga, S.A., Blanken, P.D., Noormets, A., Sulman, B.N., Scott, R.L., Wang, L., Phillips, R.P., 2016. The increasing importance of atmospheric demand for ecosystem water and carbon fluxes. Nat. Clim. Chang. 6, 1023–1027. https://doi.org/10.1038/nclimate3114.

O'Neill, P.E., Chan, S., Njoku, E.G., Jackson, T., Bindlish, R., 2016a. SMAP Enhanced L3 Radiometer Global Daily 9 km EASE-Grid Soil Moisture. [Indicate subset used]. NASA National Snow and Ice Data Center Distributed Active Archive Center, Boulder, Colorado USA. https://doi.org/10.5067/ZRO7EXJ8O3XI. [1/7/2017]. Version 1.

O'Neill, P.E., Chan, S., Njoku, E.G., Jackson, T., Bindlish, R., 2016b. SMAP L3 Radiometer Global Daily 36 km EASE-Grid Soil Moisture, Version 4. [Indicate subset used]. Boulder, Colorado USA. NASA National Snow and Ice Data Center Distributed Active Archive Center. doi: http://dx.doi.org/10.5067/OBBHQ5W22HME. [1/7/2017]. [Indicate subset used] In: SMAP L3 Radiometer Global Daily 36 km EASE-Grid Soil Moisture. NASA National Snow and Ice Data Center Distributed Active Archive Center, Boulder, Colorado USA. https://doi.org/10.5067/OBBHQ5W22HME. [1/7/2017] Version 4.

Oliphant, A.J., Grimmond, C.S.B., Zutter, H.N., Schmid, H.P., Su, H.-B., Scott, S.L., Offerle, B., Randolph, J.C., Ehman, J., 2004. Heat storage and energy balance fluxes for a temperate deciduous forest. Agric. For. Meteorol. 126, 185–201. https://doi.org/10.1016/j.agrformet.2004.07.003.

Oliva, R., Daganzo-Eusebio, E., Kerr, Y.H., Mecklenburg, S., Nieto, S., Richaume, P., Gruhier, C., 2012. SMOS radio frequency interference scenario: status and actions taken to improve the RFI environment in the 1400-1427-MHZ passive band. IEEE Trans. Geosci. Remote Sens. 50, 1427–1439. https://doi.org/10.1109/TGRS.2012.2182775.

Padilla, F.M., Pugnaire, F.I., 2007. Rooting depth and soil moisture control Mediterranean woody seedling survival during drought. Funct. Ecol. 21, 489–495. https://doi.org/10.1111/j.1365-2435.2007.01267.x.

Piepmeier, J.R., Johnson, J.T., Mohammed, P.N., Bradley, D., Ruf, C., Aksoy, M., Garcia, R., Hudson, D., Miles, L., Wong, M., 2014. Radio-frequency interference mitigation for the soil moisture active passive microwave radiometer. IEEE Trans. Geosci. Remote Sens. 52, 761–775. https://doi.org/10.1109/TGRS.2013.2281266.

Poulter, B., Frank, D., Ciais, P., Myneni, R.B., Andela, N., Bi, J., Broquet, G., Canadell, J.G., Chevallier, F., Liu, Y.Y., Running, S.W., Sitch, S., van der Werf, G.R., 2014. Contribution of semi-arid ecosystems to interannual variability of the global carbon cycle. Nature 509, 600–603. https://doi.org/10.1038/nature13376.

Poyatos, R., Granda, V., Molowny-Horas, R., Mencuccini, M., Steppe, K., Martínez-Vilalta, J., 2016. SAPFLUXNET: towards a global database of sap flow measurements. Tree Physiol. 36, 1449–1455. https://doi.org/10.1093/treephys/tpw110.

Priestley, C., Taylor, R., 1972. On the assessment of surface heat flux and evaporation using large-scale parameters. Mon. Weather Rev. 81–92. https://doi.org/10.1175/1520- 0493.

Purdy, A.J., 2018. Improvements to and Applications of Remotely Sensed Evapotranspiration. Univ. California, Irvine.

Purdy, A.J., Fisher, J.B., Goulden, M.L., Famiglietti, J.S., 2016. Ground heat flux: an analytical review of 6 models evaluated at 88 sites and globally. J. Geophys. Res. Biogeosci. 121, 3045–3059. https://doi.org/10.1002/2016JG003591.

Qiu, J., Crow, W.T., Nearing, G.S., 2016. The impact of vertical measurement depth on the information content of soil moisture for latent heat flux estimation. J. Hydrometeorol. 17, 2419–2430. https://doi.org/10.1175/JHM-D-16-0044.1.

Rodell, M., McWilliams, E.B., Famiglietti, J.S., Beaudoing, H.K., Nigro, J., 2011. Estimating evapotranspiration using an observation based terrestrial water budget. Hydrol. Process. 25, 4082–4092. https://doi.org/10.1002/hyp.8369.

Ryu, D., Famiglietti, J.S., 2005. Characterization of footprint-scale surface soil moisture variability using Gaussian and beta distribution functions during the Southern Great Plains 1997 (SGP97) hydrology experiment. Water Resour. Res. 41, 1–13. https://doi.org/10.1029/2004WR003835.

Schenk, H.J., Jackson, R.B., 2002. Rooting depths, lateral root spreads and belowground aboveground allometries of plants in water limited ecosystems. J. Ecol. 480–494. https://doi.org/10.1046/j.1365-2745.2002.00682.x.

Scott, Russell, 2017a. AmeriFlux US-SRG Santa Rita Grassland. https://doi.org/10.17190/AMF/1246154.

Scott, Russell, 2017b. AmeriFlux US-SRM Santa Rita Mesquite. https://doi.org/10.17190/AMF/1246104.

Scott, Russell, 2017c. AmeriFlux US-Wkg Walnut Gulch Kendall Grasslands. https://doi.org/10.17190/AMF/1246112.

Scott, Russell, 2017d. AmeriFlux US-Whs Walnut Gulch Lucky Hills Shrub. https://doi.org/10.17190/AMF/1246113.

Simard, M., Pinto, N., Fisher, J.B., Baccini, A., 2011. Mapping forest canopy height globally with spaceborne lidar. J. Geophys. Res. Biogeosci. 116. https://doi.org/10.1029/2011JG001708.

Sorooshian, S., Li, J., Hsu, K.L., Gao, X., 2011. How significant is the impact of irrigation on the local hydroclimate in Californias Central Valley? Comparison of model results with ground and remote-sensing data. J. Geophys. Res. Atmos. 116. https://doi.org/10.1029/2010JD014775.

Su, Z., 2002. The surface energy balance system (SEBS) for estimation of turbulent heat fluxes. Hydrol. Earth Syst. Sci. 6, 85–100. https://doi.org/10.5194/hess-6-85-2002.

Syed, T.H., Famiglietti, J.S., Chambers, D.P., Willis, J.K., Hilburn, K., 2010. Satellite-based global-ocean mass balance estimates of interannual variability and emerging trends in continental freshwater discharge. Proc. Natl. Acad. Sci. 107, 17916–17921. https://doi.org/10.1073/pnas.1003292107.

Talsma, C.J., Good, S.P., Jimenez, C., Martens, B., Fisher, J.B., Miralles, D.G., McCabe, M.F., Purdy, A.J., 2018. Partitioning of evapotranspiration in remote sensing-based models. Agric. For. Meteorol. https://doi.org/10.1016/j.agrformet.2018.05.010.

Twine, T.E.E., Kustas, W.P.P., Norman, J.M.M., Cook, D.R.R., Houser, P.R.R., Meyers, T.P.P., Prueger, J.H.H., Starks, P.J.J., Wesely, M.L.L., 2000. Correcting eddy-covariance flux underestimates over a grassland. Agric. For. Meteorol. 103, 279–300. https://doi.org/10.1016/S0168-1923(00)00123-4.

van Diepen, C.A., Wolf, J., van Keulen, H., Rappoldt, C., 1989. WOFOST: a simulation model of crop production. Soil Use Manag. 5, 16–24. https://doi.org/10.1111/j.

1475-2743.1989.tb00755.x.
Vecchi, G.A., Wittenberg, A.T., 2010. El Niño and our future climate: where do we stand? Wiley Interdiscip. Rev. Clim. Chang. 1, 260–270. https://doi.org/10.1002/wcc.33.
Vinukollu, R.K., Wood, E.F., Ferguson, C.R., Fisher, J.B., 2011. Global estimates of evapotranspiration for climate studies using multi-sensor remote sensing data: evaluation of three process-based approaches. Remote Sens. Environ. 115, 801–823. https://doi.org/10.1016/j.rse.2010.11.006.
Wang, K., Dickinson, R.E., 2012. A review of global terrestrial evapotranspiration: observation. J. Geophys. Res. Lett. https://doi.org/10.1029/2011RG000373.1.
INTRODUCTION.
Wood, Jeffrey, Gu, Lianhong, 2017. AmeriFlux US-MOz Missouri Ozark Site. https://doi.org/10.17190/AMF/1246081.
Zreda, M., Desilets, D., Ferré, T.P.A., Scott, R.L., 2008. Measuring soil moisture content non-invasively at intermediate spatial scale using cosmic-ray neutrons. Geophys. Res. Lett. 35. https://doi.org/10.1029/2008GL035655.
Zreda, M., Shuttleworth, W.J., Zeng, X., Zweck, C., Desilets, D., Franz, T., Rosolem, R., 2012. COSMOS: the cosmic-ray soil moisture observing system. Hydrol. Earth Syst. Sci. 16, 4079–4099. https://doi.org/10.5194/hess-16-4079-2012.